Eur. Phys. J. D **44**, 187–200 (2007)
DOI: 10.1140/epjd/e2007-00177-6

THE EUROPEAN PHYSICAL JOURNAL D

Coherent harmonic generation on UVSOR-II storage ring

M. Labat[1,a], M. Hosaka[2], A. Mochihashi[2], M. Shimada[2], M. Katoh[2], G. Lambert[3], T. Hara[3], Y. Takashima[4], and M.E. Couprie[5]

[1] CEA Saclay (DSM/DRECAM/SPAM), Bâtiment 522, 91191 Gif-sur-Yvette, France
[2] UVSOR, Institute for Molecular Science, Myodaiji, Okazaki 444, Japan
[3] RIKEN SPring-8 Harima, 1-1-1 Kouto, Sayo-cho, Sayo-gun Hyogo 679-5198, Japan
[4] Nagoya University, Furo-cho, Chikusa-ku, Nagoya 464-8603, Japan
[5] Synchrotron SOLEIL, Saint Aubin, B.P. 34, 91192 Gif-sur-Yvette, France

Received 9 January 2007
Published online 1st June 2007 –

Abstract. Among the attractive coherent light sources resulting from the interaction between femtosecond lasers and relativistic electron beams, simultaneous Coherent Synchrotron Radiation (CSR) in the THz region, slicing and UV-VUV Coherent Harmonic Generation (CHG) can be achieved on synchrotron radiation facilities. Recently, a Ti:Sa laser at high repetition rate (1 kHz) has been seeded in the optical klystron of the Free Electron Laser at UVSOR-II (Okazaki, Japan). In this paper, the experimental set-up allowing delivery of sub picosecond UV pulses from CHG, and TeraHertz radiation from CSR is described. We further focus on the third coherent harmonic (266 nm) generated. The expected typical characteristics of this radiation, predicted by both numerical and analytical models recalled here, are experimentally verified and several studies of the influence of the seed laser on the output CHG intensity are reported. Such experiment enables UVSOR-II facility to produce in parallel short pulses at two different colors, synchronized at high repetition rate with one single infrared laser: a unique set-up of great interest for the facility users.

PACS. 41.60.Cr Free-electron lasers – 42.65.Ky Frequency conversion; harmonic generation, including higher-order harmonic generation – 29.27.-a Beams in particle accelerators

Highlight Paper

1 Introduction

Future light sources now aim at producing short pulses (femtosecond scale) from ultrashort (below 1 nm) to very long (in the mm range) wavelengths opening new areas in various scientific domains [1,2]. Ultrashort femtosecond pulses enable direct measurement of, e.g., molecular dynamics on the time scale of a vibrational period in the gas phase, or the atomic motion and structural changes in the condensed phase. The extension to sub nm wavelengths is of major interest since such radiations can excite the core electrons in atoms, providing information on the atomic positions and bond lengths. TeraHertz radiations, i.e. mm wavelengths, will serve to imaging and spectroscopy, to explore physical properties of materials. The interaction of an intense laser with a relativistic electron beam is one of the possible schemes for generating femtosecond pulses in the sub-nm and mm-wavelength range.

The Thomson scattering [3] of a femtosecond laser beam by relativistic synchrotron electron bunches has enabled generation of 300 fs X-ray pulses [4]. At SPring-8, gamma-rays have been produced by laser Compton scattering using a far-infrared laser [5]. At ESRF, gamma-rays obtained by Compton backscattering of photons from the circulating electrons are used for studies in nuclear and particle physics [6]. The slicing technique [7], another scheme to achieve femtosecond VUV to X-ray pulses [8], consists of an ultrashort and intense laser pulse which modulates with high amplitude the energy of a slice in the electron bunch. The slice, further separated from the rest of the longitudinal distribution and driven through an appropriate undulator produces X-rays with approximately the same duration as the laser pulse. When such a scheme is applied to storage ring, sub-ps pulses can be delivered to users instead of the usual tens-ps ones, due to recirculation of the electron bunch. Coherent Synchrotron Radiation (CSR) [9] is observed when the electronic longitudinal distribution becomes shorter than the radiation wavelength of the bunch, and leads to production of TeraHertz pulses [10–13]. This can be achieved with a significant reduction of the bunch length, or in presence of a microstructure within the bunch. Laser created microstructures (using the same slicing technique previously mentioned), led to generation of femtosecond TeraHertz radiation at BESSY [11].

[a] e-mail: marie.labat@synchrotron-soleil.fr

Free Electron Lasers [14], based on the amplification of the spontaneous emission of a relativistic electron beam, already cover an extended spectral range from microwaves [15] to soft X-rays pulses [16] in sub-picosecond regime [16]. The relativistic electron beam, provided by an accelerator (a storage ring or a linear accelerator for instance) is driven through an undulator, a periodic permanent magnetic structure, making the electrons wiggle around a longitudinal axis and radiate at the resonant wavelength. In the oscillator, i.e., multi-pass configuration [14,17], the radiation is stored in an optical cavity and amplified until saturation after successive passes of the electron bunches in the cavity. The output wavelength is limited on VUV side by the available mirrors for the cavity. In the single-pass configuration, such as Self Amplified Spontaneous Emission (SASE) [18], saturation is reached by implementing a large number of undulator sections: the spontaneous emission emitted in the first undulator sections gradually starts to grow exponentially thanks to the interaction with the electron beam. SASE is today the dominant scheme to achieve X-rays. However, its output has a limited temporal coherence and displays important intensity fluctuations. As an alternative to both oscillator and single-pass configurations, seeding Free Electron Lasers has been proposed to produce temporally coherent, stable, short wavelength pulses, and to achieve shorter saturation lengths for single-pass FELs. In the seeded configuration [19,21], the electrons act as a non-linear medium radiating harmonics of a seed source (e.g., a laser). In the two-step seeding scheme, the seed field forces an energy modulation on the electron bunch in a short undulator called the modulator. The resonant frequency of this modulator is tuned to the seed wavelength. This energy modulation is then converted into a density modulation — microbunching — as the electron beam travels through a dispersive section. Finally, in a second undulator called the radiator, the microbunched electron beam can emit coherently at the fundamental and the harmonics of the seed source. The amplified wavelength is selected by tuning the radiator resonant wavelength. The seed can be either an external source or the FEL pulse itself. As an external seed at very short wavelength, high order harmonics of a laser generated in gas have been recently proposed [23]. On linear accelerator based FELs operating in the high gain regime, the seeded configuration is usually referred to as High Gain Harmonic Generation (HGHG, where the second undulator is tuned at one of the harmonics of the fundamental) [24], whereas for FELs operating in lower gain regime, it is referred to as Coherent Harmonic Generation.

The first experimental demonstration of Coherent Harmonic Generation was performed on ACO storage ring [25], using an external Nd:YAG laser focused in an optical klystron — two undulators separated by a dispersive section [26]. The third harmonic (354.7 nm) of the fundamental wavelength (1064.1 nm) was observed, as well as the third and fifth harmonics (177 and 106.4 nm) of the doubled laser. Similar results were obtained on Super-ACO [27] storage ring, using the same seed. At BNL, the HGHG FEL seeded by Ti:Sa laser at 800 nm, delivered saturated amplified third harmonic (266 nm) [28]. The seventh harmonic (88 nm) has even been used in a chemistry experiment [29]. Duke and ELETTRA storage rings demonstrated the CHG configuration seeding with the FEL pulse itself. The third harmonic (221.8 nm) of giant pulse at 665.4 nm was observed at Duke [30], as well as, in further VUV experiments, the second to seventh (118 to 37 nm) harmonics of giant pulse at 236 nm. At ELETTRA [31], the Q-switched FEL pulse at 660 nm allowed generation of third harmonic at 220 nm, and CHG experiments using an external infra-red seed laser are about to start [32].

In this paper, we report CHG experiment performed at 1 kHz repetition rate on the UV-FEL of UVSOR-II storage ring [33] in parallel with CSR experiments. An external, kHz repetition rate, femtosecond infra-red laser is injected in an optical klystron, leading by CHG to the generation of sub-picosecond UV pulses. The high repetition rate is one major specificity of our work. In addition, one single external laser leads to both CHG in the UV range and CSR producing TeraHertz radiation. The two radiations, collected in different locations, are synchronized with the laser and can be combined: this offers a very attractive and unique multi-color source for, e.g., pump-probe studies in several fields.

In Section 2, we first present the models for understanding Coherent Harmonic Generation process: an analytical and a numerical model. In Section 3, we describe the experimental set-up, and in Section 4, we report the demonstration of Coherent Harmonic Generation. Section 5 is finally dedicated to the dependency of the third coherent harmonic intensity under several laser parameters.

2 Analytical and numerical models for coherent harmonic generation

Coherent Harmonic Generation in an optical klystron was first understood using a one dimensional analytical model [20,21]. Numerical model further helped introducing additional parameters such as time dependency and beam longitudinal distribution.

2.1 Analytical model

In the analytical model, developed by Coïsson and De Martini [21], the relativistic motion of the electrons under both the magnetic field of the undulators and the seed electric field — here a laser field assumed as a plane wave — obeys the Lorentz equations, leading to the simple pendulum model equations [22] for their energy and phase evolution. Assuming that the initial conditions (in normalized energy γ and phase ϕ_0 in the longitudinal distribution) remain constant along the first undulator in the planar configuration, the variation of the energy output is

given by:

$$\frac{\delta\gamma}{\gamma} = \frac{eKNE_{Laser}\lambda_0}{2\gamma^2 mc^2}(J_0(\xi) - J_1(\xi))\sin(\phi_0). \quad (1)$$

In (1), E_{Laser} is the peak laser electric field:

$$E_{Laser} = \left[\frac{2P_{Laser}}{f\sqrt{2\pi}\sigma_{Laser}c\epsilon_0\pi^{3/2}w_0^2}\right]^{1/2}, \quad (2)$$

with P_{Laser} the average power, f the repetition rate, w_0 the waist, and σ_{Laser} the rms pulse width of the laser, $J_{0,1}$ are Bessel functions of order 0 and 1, depending on $\xi = K^2/(4(1+K^2/2))$, K is the undulator deflection parameter, λ_0 the spatial period, N the number of periods, c the velocity of light, ϵ_0 the permittivity of free space, e and m the electron charge and mass. Along the dispersive section, the energy variation induced results into a phase shift $\delta\alpha$ of the electrons, equal to:

$$\delta\alpha = 4\pi(N + N_d)\frac{\delta\gamma}{\gamma}, \quad (3)$$

where N_d is the number of undulator equivalent periods of the dispersive section. The electrons gather in microbunches separated in the phase space by 2π, creating a modulated electronic density at the entrance of the second undulator.

The spontaneous emission I_{OK} produced by one electron in an optical klystron results from the interference of its radiation I_{und} in each undulator [34]: $I_{OK} = 2I_{und}(1+\cos(\alpha))$, α being the phase difference between the two radiations. The total emission produced by the whole electron bunch consists in two terms, referred to as coherent and incoherent, respectively given by [35]:

$$I_{coh} = I_{und}N_e^2 f_n^2 J_n^2(n\Delta\alpha) \quad (4)$$

$$I_{incoh} = 2I_{und}N_e(1 + f_n J_0(n\Delta\alpha)), \quad (5)$$

where $f_n = e^{-8(n\pi(N+N_d)\sigma_\gamma)^2}$ is the modulation rate [34], $\Delta\alpha$ the maximum phase shift defined for maximum energy modulation $(\delta\gamma/\gamma)_{max}$ (at $\phi_0 = 0$), and N_e the number of electrons in the bunch. Whereas a random phase distribution for the bunch averages to zero the coherent term, a modulated distribution enhances it.

In this model, the whole electronic distribution is assumed to be modulated by the laser, and the energy transfer between electrons and photons to be loss free. Since the longitudinal and transverse dimensions of the laser pulse are very different from those of the electron bunch, and considering that the electrons wiggle around the laser path, modifications have been introduced to the above model.

The filling factor F_f [36] calculated by Colson and Elleaume [37] can provide an analytical evaluation of the transverse overlap between the photon and the electronic beams in an undulator, taking into account the Gaussian profile of the laser, and the wiggling of the electrons. It was initially introduced in the gain calculation of an FEL resonator [37], i.e., in the energy transfer calculation between the electrons and the photons. Its empirical analytical expression is given by [38]:

$$F_f = \frac{\sqrt{aW_x}}{(1+bW_x^2)\sqrt{1+\frac{c}{\Sigma_x^2}}}\frac{\sqrt{aW_y}}{(1+bW_y^2)\sqrt{1+\frac{c}{\Sigma_y^2}}}, \quad (6)$$

where a, b, and c are constants evaluated with numerical fit, $\Sigma_{x,y} = \sigma_{x,y}\sqrt{\pi/(\lambda_{Laser}L_{und})}$, $W_{x,y} = w_{x,y}\sqrt{\pi/(\lambda_{Laser}L_{und})}$ with $\sigma_{x,y}$ the transverse rms dimensions of the electron beam, $w_{x,y}$ the waist of the seeding laser, λ_{Laser} its wavelength, and L_{und} the first undulator length. Since the small signal gain, derived from Madey second theorem [39], is proportional to the energy exchange at the second order, i.e. to the energy derivative of the squared energy shift $\delta\gamma/\gamma$, the filling factor is used to correct the energy modulation given by the initial model according to: $(\delta\gamma/\gamma)_{corr} = \sqrt{F_f}\delta\gamma/\gamma$, leading to the maximum corrected phase shift:

$$\Delta\alpha = 4\pi(N + N_d)\sqrt{F_f}\left(\frac{\delta\gamma}{\gamma}\right)_{max}. \quad (7)$$

Today, thanks to the Chirp Pulse Amplification (CPA) [40], femtosecond pulse duration lasers are common systems. On the other hand, the length σ_e of the stored electron bunches remains of several picoseconds, that is several orders of magnitude longer than the laser pulse duration. As a consequence, in experiments such as slicing, CSR or CHG, the interaction is localized in a very narrow slice of the bunch, of length σ_{Laser}, containing $N_{e-L} = (\sigma_{Laser}/\sigma_e)N_e$. The coherent term can then be approximated by:

$$\begin{aligned} I_{coh} &= I_{und}N_{e-L}^2 J_n^2(n\Delta\alpha) \quad (8)\\ &= I_{und}N_e^2\left(\frac{\sigma_{Laser}}{\sigma_e}\right)^2 J_n^2(n\Delta\alpha), \end{aligned}$$

and the incoherent term, coming from the $N_e - N_{e-L}$ non-interacting electrons (the incoherent emission of the N_{e-L} interacting electrons is negligible), by:

$$\begin{aligned} I_{incoh} &= 2I_{und}(N_e - N_{e-L})(1 + f_n J_0(n\Delta\alpha)) \quad (9)\\ &= 2I_{und}N_e\left(1 - \frac{\sigma_{Laser}}{\sigma_e}\right)(1 + f_n J_0(n\Delta\alpha)). \end{aligned}$$

The above analytical model highlights the main steps of CHG from an external seed laser and helps understanding the whole process. Nevertheless, this model is steady-state and one-dimensional, and therefore it doesn't provide any information neither on the dynamics of the electron beam (refreshment between two laser shots [41], evolution in the phase space), nor on the spectral domain. To investigate further, a numerical model is used.

2.2 Numerical model

PERSEO Time Dependent version [42] performs simulation of the FEL dynamics in a wide range of configurations: oscillator FEL, seeded FEL, cascaded FEL... It is used here to analyze CHG.

In this numerical model, the ith particle of the relativistic electron beam is described with the phase space variables (θ_i,ν_i), where θ_i is the electron phase corresponding to its longitudinal position along the bunch, and ν_i its frequency shift referred to the reference frequency (for which the energy exchange is null).

The FEL electric field is a superposition of slowly varying complex amplitudes $|a_n|e^{i\phi_n}$ for each harmonic n:

$$E(z,t) = \sum_n \tilde{E_n}|a_n|e^{i(k_n z - \omega_n t + \phi_n)}. \quad (10)$$

The parameters $\tilde{E_n}$ weighting the field amplitude on the nth harmonic, with k_n its wavevector and ω_n its optical frequency, depend on the saturation intensity $I_s(n)$ as $\tilde{E_n} = \sqrt{z_0 I_s(n)/(4\pi)}$, z_0 being the vacuum impedance. The initial electric field corresponds either to spontaneous emission, shot noise, or to an input seed such as an external laser.

The particle motion is ruled by the pendulum-like equations:

$$\begin{cases} \dfrac{d\theta_i}{d\tau} = \nu_i \\ \dfrac{d\nu_i}{d\tau} = \sum_n \cos(n\theta_i)\mathrm{Re}(a_n) - \sin(n\theta_i)\mathrm{Im}(a_n). \end{cases} \quad (11)$$

The evolution of the amplitudes a_n is governed by:

$$\begin{cases} \dfrac{\partial \mathrm{Re}(a_n)}{\partial \tau} = -2\pi g_n \langle \cos(in\theta_i(\tau)) \rangle_i \\ \dfrac{\partial \mathrm{Im}(a_n)}{\partial \tau} = -2\pi g_n \langle \sin(in\theta_i(\tau)) \rangle_i, \end{cases} \quad (12)$$

where τ is the normalized time, g_n the coupling coefficients [43] which depend on the electron beam dimensions and charge, and on the undulator parameters.

Resolution of the coupled equations (11) and (12) provides the output radiation electric field as well as the corresponding particle phase space distribution. In this single-pass calculation, the recirculation of the electron beam is not modeled. According to preliminary simulations using SYNC code [41] and to first experimental results, the refreshment of the electron beam seems to occur in between two laser shots, and therefore the relaxation time to be shorter than the synchrotron damping time allowing single-pass approximation. As a consequence, information on the refreshment of the phase space cannot be retrieved. Still, PERSEO parameterized in CHG configuration allows simulation of the third harmonic spectral power, longitudinal distribution, and visualization of the electronic phase space throughout its interaction with the seed laser. The expected performances and dependencies will be compared to the experimental results in the following sections.

3 Experimental set-up

3.1 Electron beam

In CHG operation, UVSOR-II facility operated in the single bunch mode provides an electron beam which main characteristics are given in Table 1. Up to 40 mA of beam current (I) can be stored in the ring without any vertical beam instability (above this value, transverse instabilities can be neutralized by tuning the chromaticity). Since the successful upgrade in 2003 [44] (which allowed reduction of the emittance by factor 6, and therefore higher brilliance in the insertion devices), the storage ring can be set either in chromatic or achromatic configuration: non null or null dispersion function in the optical klystron. The corresponding magnetic functions are presented in Table 1. In the experiments reported here, chromatic optics were used.

Table 1. Characteristics of the electron beam on UVSOR-II storage ring for CHG operation.

Parameter	Symbol	Value
Energy (MeV)	E	600
Circumference of the Ring (m)	C	53.2
Cavity voltage (kV)	V_{RF}	100
RF frequency (MHz)	f_{RF}	90.1
Harmonic number	n_H	16
Number of bunches stored	n_b	1
Period of revolution (ns)	T_0	178
Frequency of revolution (MHz)	f_{rev}	5.6
Momentum compaction	α_c	0.028
Synchrotron frequency (kHz)	f_S	19.4
Damping time (ms)	τ_S	20
Beam Current (mA)	I	0–40
Dispersive function in OK (m)	η	0.8 / 0
Natural energy spread (10^{-4})	σ_γ	3.4
Total emittance (nm rad)	ϵ	17.5 / 38
Transverse dimensions in OK		
horizontal (μm)	σ_X	500 / 550
vertical (μm)	σ_Y	28 / 38
Coupling assumed	(%)	3

Because of the potential well distortion [45,46], the bunch length increases with current: it is 84 rms-ps at 1 mA, and reaches 117 rms-ps at 33 mA. The bunch length is deduced from the longitudinal distribution of the electron beam radiation, measured with a double sweep streak camera (Hamamatsu, C5680).

3.2 Optical klystron

At each turn, the electron beam passes through a planar to helical optical klystron (see Tab. 2), UNKO-3 installed since 1997 [47,48]. The initial configuration of the undulator consists of a 21 periods magnet array of three lanes. Center lane and side lanes provide respectively vertical and horizontal magnetic fields. In the Optical Klystron (OK) configuration, the three central periods are replaced by another set of magnets to create a dispersive section providing a wide wiggle of magnetic field. By shifting the lanes, the phase between the magnetic fields can be changed, allowing to achieve planar, ellipsoidal as well as complete helical polarizations with both ellipticities.

The magnetic functions inside the OK ($\beta_{x,z}$, and η) set the electrons orbit: a sinusoidal or helicoidal trajectory

Table 2. Characteristics of the optical klystron.

Parameter	Value
Number of period per undulator	9
Spatial period of the undulators (cm)	11
Length of the dispersive section (cm)	33
Gap range (mm)	30–230
K deflection parameter	$\leq$6.9 (helical)
	$\leq$8.6 (planar)
Equivalent number of periods	80–140
η in OK (m)	0 / 0.8
β_x; β_z in OK (m)	8 ; 1.3 / 10 ; 1.5
Peak magnetic field (T)	0.74531

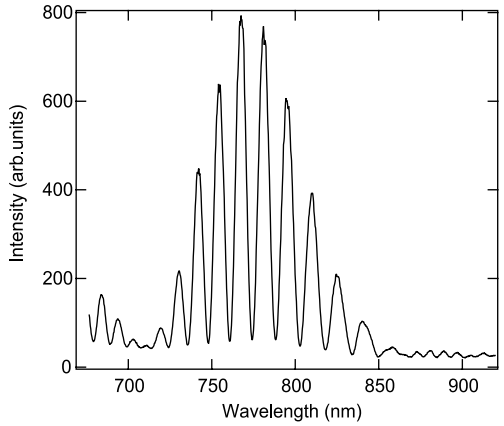

Fig. 1. Spectrum of the spontaneous emission produced in the OK. Measurement performed with a spectrometer Hamamatsu PMA-10, which measured resolution is 0.11 nm. Undulator gap = 40.8 mm, $I = 20$ mA/2 bunches (10 mA/bunch). Resonant wavelength is at 773 nm. The spectral width of the envelope of the whole spectrum (defined by $(\Delta\lambda/\lambda)_{spectrum} = 1/N$) $N = 11$. The difference with the actual value ($N = 9$) may be due to misalignment of the electronic trajectory along the two undulators. The spectral width of the fringes (defined by $(\Delta\lambda/\lambda)_{fringe} = 1/(N + N_d)$) leads to $N_d = 96$.

around a longitudinal axis as straight as possible along the two undulators. The OK spectrum presented in Figure 1 results from the interference of the radiation from the two undulators [34]. Optimisation of the orbit is performed by maximizing the fringes contrast, i.e. the modulation rate: $f = e^{-8(\pi(N+N_d)\sigma_\gamma)^2}$. The contrast gives also a measurement of the electron beam energy spread: $\sigma_\gamma = 4.2 \times 10^{-4}$.

For CHG experiments, the resonant wavelength of the OK is tuned at the seed laser wavelength in planar configuration, enabling amplification of the non linear odd harmonics of the fundamental. Operating in helical configuration would allow circularly polarized light to be delivered, a scheme that has never been tested yet, and which could offer very attractive perspectives for production on-axis of even harmonics [49].

3.3 Laser system

The input seed is provided by a femtosecond laser system at 800 nm in place since March 2005. This standard

Table 3. Characteristics of the seeding laser.

Parameter	Value
Pulse energy (mJ)	2.5
Pulse duration (FWHM-ps)	0.1 to 2
Repetition rate (kHz)	1
Wavelength (nm)	800
Beam diameter (mm-FWHM)	8
Gaussian quality factor	1.25
Polarization	horizontal

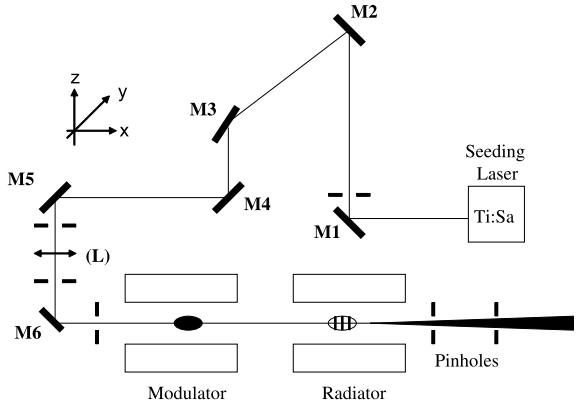

Fig. 2. Experimental set-up for the alignment procedure of the seeding laser inside the OK. All pinholes were placed using autocollimation method. The distances between the optics are: $L_{M1-M2} = 1.5$ m, $L_{M2-M3} = 4$ m, $L_{M3-M4} = 1$ m, $L_{M4-M5} = 3$ m, $L_{M5-L} = 0.5$ m, $L_{L-M6} = 0.54$ m. The couples M1–M2, M3–M4 and M5–M6 enable vertical transportation of the laser. The M2–M3 couple is for horizontal transportation. The modulator entrance is at 4.92 m from M6. M4 and M5 are used for alignment.

system is composed of a mode-locked titanium-sapphire (Ti:Sa) oscillator (Coherent, Mira 900-F, pumped by CW laser (Verdi-V5)), feeding a regenerative amplifier (Coherent, Legend HE, pumped by Q-switched laser at 1 kHz separate); the main characteristics are listed in Table 3.

Since it was initially purchased for CSR and Slicing experiments [50], the system is not fully optimised for CHG: the Fourier-transformed pulse of 100 fs duration is shorter than the electron bunch by nearly two orders of magnitude, resulting in a poor longitudinal overlap. However, introducing a chirp in the pulse permits to increase the duration until 1 ps (further controlled with an autocorrelator). Actually, with this laser system and for the first time on a storage ring, we have seeded a FEL for Harmonic Generation at high repetition rate, whereas former experiments were limited to 10 Hz [27].

3.4 Laser beam transport and alignment

The seeding laser is transported from the laser hutch to the OK using three periscopes, each consisting of two flat coated mirrors (see Fig. 2). This configuration keeps the initial horizontal polarization of the laser, matching the electronic polarization set by the undulators planar configuration. The laser beam is focused with a lens of 5.8 m

Table 4. Characteristics of the mirrors used for transport of the seeding laser.

Mirrors	M1/2	M3/4/5/6
Reference	FLM1-30C05-800	TFM-50C08-800
Diameter (mm)	30	50
Wavelength (nm)	750–850	770–840
Width (mm)	5	5
Material	B	B
Surface Flatness	(λ/10)	(λ/10)
Parallelism	$\leq$5 arcs	$\leq$3 arcmin
Reflectivity at 800 nm	$\geq$95%	$\geq$ 95%

focal length (at entrance of the vacuum chamber), so that maximum intensity is reached at the entrance of the modulator.

Optimisation of the spatial overlap between the two beams is required to maximize the electron-photon interaction. Once the magnetic axis has been defined by tuning the magnetic functions, the laser should be accurately aligned on this axis. To this purpose, the spontaneous emission in the undulator is autocollimated, i.e., sent back throughout the undulators to the laser hutch, so that its path can be tracked with several pinholes; the laser is then aligned on these pinholes (using M4 and M5 mirrors of Fig. 2). Assuming electron beam transverse dimensions of 800 μm $\times$ 45 μm at both extremities of the OK, simple calculations show that an angular accuracy of $\pm 4\,\mu$rad would be required for fine alignment, that is much higher than that of the mounts we used ($\pm 650\,\mu$rad), and somewhat higher than the laser pointing stability. Using motorized mounts or high precision screws would certainly facilitate the alignment procedure, and might improve the transverse laser/electron beam overlap.

Analytical calculation of the filling factor (see Fig. 3) shows that the transverse overlap can be further optimized by adjusting the laser waist size w_0: the filling factor is maximum for $w_0 = 600\,\mu$m whereas measured waist size is 200 μm. This could be easily adjusted by decreasing the numerical aperture, without too much reducing the laser pulse energy (using a longer focal length or afocal arrangement). The position of the waist could also be shifted towards the OK center, and the vertical dimension of the electron beam increased.

3.5 Synchronisation

Synchronisation of the seeding laser injection with the electron bunch revolution in the ring is illustrated in Figure 4. A cavity pick-up delivers, after amplification, the RF cavity signal at 90.1 MHz to a synchronous generator and to sub-harmonic generators. A feedback with the synchronous generator enables the Ti:Sa laser to deliver 130 fs pulses at the RF cavity frequency with a typical precision of $\pm$100 Hz. The two successive sub-harmonics generators divide the RF frequency until it reaches 1 kHz. This signal triggers the Pockels cell which feeds the regenerative amplifier. Both laser injection and electron bunch revolution are driven by the RF cavity signal. A phase shifter in the

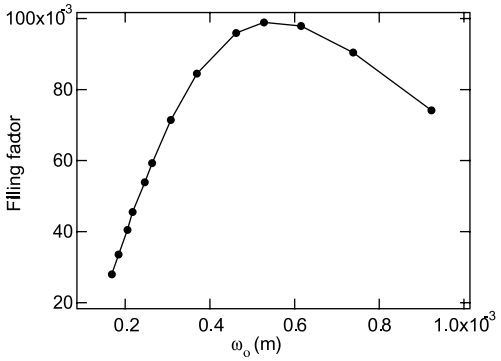

Fig. 3. Filling factor (F_f) vs. seeding laser waist at focusing point. Calculations have been performed using the parameters of Tables 1–3.

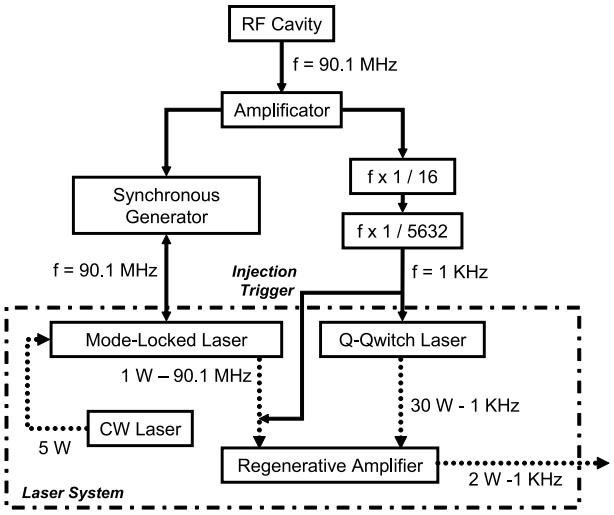

Fig. 4. Schematic diagram of the ultra-short pulse laser system and its synchronisation with the electron beam. Synchronous generator is a Synchro-Lock AP, Q-Switch Laser is an Evolution-30, Regenerative Amplifier is a Legend HE. The timing system (THAMWAY, A073-2417A) has been developed at UVSOR-II.

RF system is finally used to adjust the timing of the laser pulse within the bunch spacing time. Delay between laser pulse and spontaneous OK radiation is first monitored with a photomultiplier (Hamamatsu, R928). More accurate tuning is further performed using the double sweep streak camera (see Fig. 5).

4 Generation of the third coherent harmonic

The demonstration of laser-electron beam energy exchange, resulting in a bunch heating, is first studied as a necessary step for evidence of coherent harmonic generation.

4.1 Electron bunch heating

CHG process starts with the modulation of the electron beam inside the modulator by the seeded laser. Figure 6

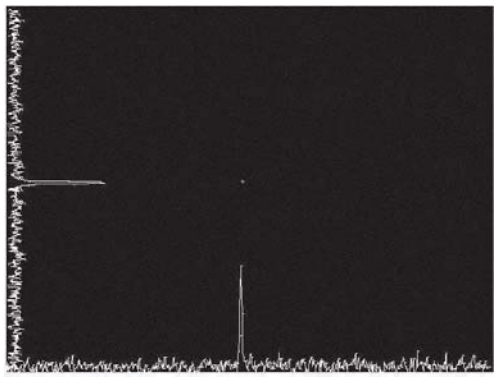

Fig. 5. Measurement of the streak camera resolution. The spatial resolution measured is 3.5 FWHM-pixels. Using the fastest sweep, i.e. shortest vertical scale of 149 ps, a temporal resolution of 1.1 FWHM-ps is allowed. With 694 ps time scale (resp. 1293, 1883 ps), it is 4.7 FWHM-ps (resp. 8.8, 12.9 FHWM-ps).

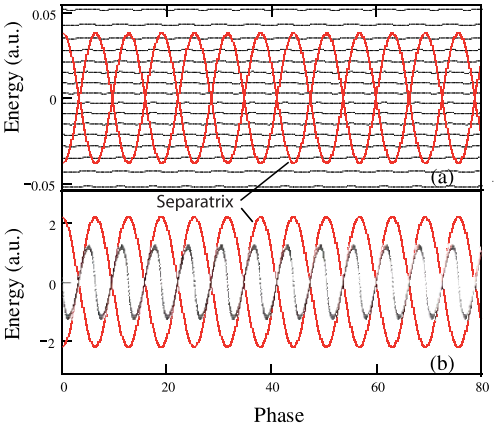

Fig. 6. Phase space of the electrons at the modulator output simulated with PERSEO code. (a) Without laser injection, (b) with laser injection: $P_{seed} = 1.17$ GW (corresponding to an average power of 1.5 W). The separatrix of the motion is proportional to the square root of the field. Parameters for the simulation: $\epsilon_n = 1$ mm mrad (normalized emittance), $\sigma_\gamma = 4.2\times10^{-4}$, $\sigma_{laser} = 512$ fs, and parameters of Tables 1–3. Peak power is used for the seeding power definition.

illustrates the simulated phase space of the particles at the end of the modulator. The energy modulation without laser injection remains low: bunching coefficient on the fundamental and on the third harmonic are below 2.5×10^{-3}. With a gain length of 2.45 m, the undulator itself cannot lead to saturation, or even significant third harmonic production. With laser injection, the phase space is drastically modified: the energy distribution gets modulated. Seeding with 0.5 W and 1200 fs pulse duration increases the bunching coefficient up to 0.25 on the fundamental, and to 0.05 on the third harmonic. With those parameters, a 4.2 nJ energy pulse on the third harmonic is expected, allowing optimistic perspectives for CHG experiment.

The electron bunch revolution period is 178 ns, whereas laser injection period is 1 ms, allowing refreshment of the bunch during the 5617 turns between two

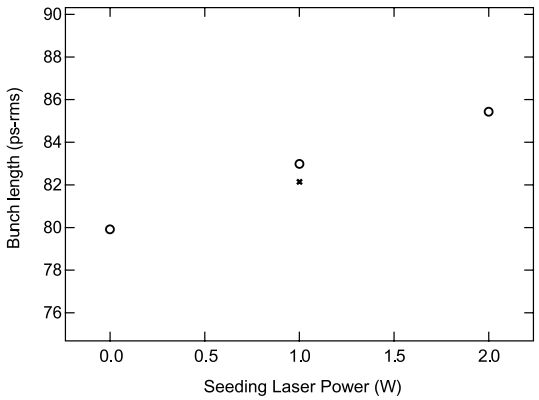

Fig. 7. Electron bunch length versus seeding laser average power. (○) $\Delta T_{Laser} = 560$ fs, (×) $\Delta T_{Laser} = 180$ fs. Measurement performed with the double sweep streak camera using 100 ms for horizontal scale and 1400 ps for vertical scale. $I = 1.45$ mA.

seedings. For each seeding, the laser induces a heating of the electrons interacting with its electric field, i.e. a small portion of the electronic distribution. These heated electrons are then refreshed along the entire distribution via the synchrotron damping process. The bunch length is correlated to the energy spread via its theoretical expression in a storage ring [51]: $\sigma_e = (\alpha_c/2\pi f_s)\sigma_\gamma$. One would then expect, looking at the bunch length evolution in time, an increase due to heating, followed by a decrease corresponding to refreshment.

The bunch length measured as a function of the seeding laser power is presented in Figure 7. Without laser injection, the electron bunch length is 80 ps. Seeding with 1 W of average power causes an enhancement by 4% (corresponding to 83 ps), and by 7.5% with 2 W (corresponding to 85.4 ps). As expected, seeding induces an energy modulation of the beam resulting into an increase of the energy spread and a further bunch lengthening. But, because of the limited resolution of the double sweep streak camera, no significant variation of the bunch length could be detected in between two laser injections: the refreshment might occur within less than a few tens of μs. The electronic longitudinal distribution reaches an equilibrium which characteristics (bunch length, energy spread) depend on the seeding laser parameters. According to Figure 7, the higher the seeding laser power, and the pulse duration, the higher the bunch length and therefore the equilibrium energy spread.

The analytical model gives an expression of the energy modulation induced by the laser on one heated electron depending on its phase relative to the laser field. It does not provide the final energy distribution, i.e. the energy spread that can be experimentally measured. Nevertheless, one can still notice a qualitative agreement between experimental results and the analytical model. Indeed, the higher the laser electric field, the higher the maximum energy modulation of the electrons in the modulator (given by the model), and the more intense is the coherent emission, using for calculations the parameters given in Section 3 and a filling factor below 0.01.

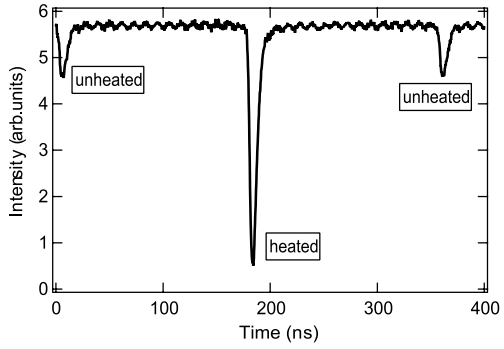

Fig. 8. Electron bunch emission vs. time. The OK output radiation is sent through an interferometric filter (CVI-F25-265) centered at 265 nm with 25 nm bandwidth for spectral selection. A 40 mm focusing silica lens collects the entire UV beam and focuses it to a solar blind PhotoMultiplier (PM, Hamamatsu, R759). To avoid saturation of the detector, UV absorption densities are used, calibrated with a Hg lamp and a monochromator tuned at 266 nm. PM signal is then sent to an oscilloscope triggered by the laser system. Central peak corresponds to the laser heated bunch emission, and edged peaks to unheated bunch emission. The electron bunch experiences one laser shot every 5682 turns. $P_{Laser} = 1.12$ W, $\Delta T_{Laser} = 1.12$ ps, $I = 2.43$ mA.

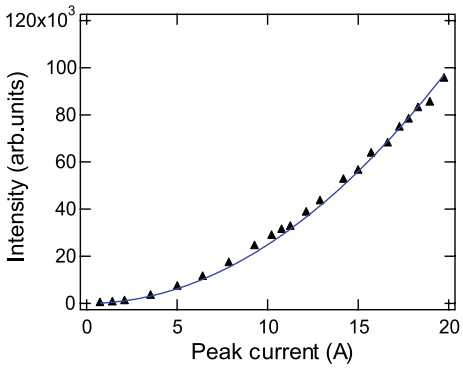

Fig. 9. Coherent emission on the third harmonic versus peak current. (▲) The coherent emission is assumed to be the difference between the electron bunch heated signal and the unheated one. The measurement is similar to the one detailed in the caption of Figure 8. Solid line is the quadratic fit function. $E_{Laser} = 1.7$ W, $\Phi_{Laser} = 8$ mm (before focusing lens), $\Delta_{Laser} = 840$ ps.

Figure 7 also shows that shorter laser pulse duration leads to smaller bunch lengthening at the given average power of 1 W, in agreement with the prediction of the analytical model. An increase of the pulse duration reduces the peak power of the laser, and therefore the local maximum energy modulation. On the other hand, it improves the longitudinal overlap between the two distributions, involving more electrons in the interaction.

The bunch lengthening observed is an evidence of the energy modulation performed by the laser within the coherent harmonic generation process.

4.2 Coherent third harmonic generation

Figure 8 illustrates the electron bunch emission at the output of the OK along three revolution periods in the storage ring. Central peak, synchronised on the laser signal, corresponds to the laser heated bunch emission at 266 nm, i.e. on the third harmonic of the resonant wavelength. The two edge peaks, separated each by one revolution period (178 ns) from the central peak, correspond to spontaneous emission of the unheated bunch (one loop before, and one loop after laser shot). The central peak is 4 times more intense than the edge ones. The microbunching induced by the seeding laser results into an additional emission on the third harmonic of the fundamental laser wavelength, corresponding to the coherent term I_{coh} in the analytical model. The energy of the coherent emission can be estimated using calculations with SPECTRA [52] of the spontaneous emission. At 2.43 mA beam current, the calculated energy of the spontaneous emission pulse on the detector, taking into account the response of the filter and the spectral width of the spontaneous emission, is 4.37 pJ. Assuming the measured enhancement by a factor 4 at this beam current, the estimated energy of the coherent third harmonic on the detector is 17.5 pJ, corresponding to 65 W of peak power at the output of the OK, i.e. before filter.

To further confirm the observation of coherent harmonic generation, the intensity of the third harmonic is measured as a function of the beam current. Laser heated bunch emission is no longer proportional to the beam current: it increases faster. Around 30 mA, the signal is 10 times more intense with laser injection than without it. The additional signal of the heated electron bunch emission with respect to spontaneous emission, has been plotted as a function of the peak current (see Fig. 9). Indeed, the number of electrons heated by the laser, N_{e-L}, is proportional to the electronic density around the center of the bunch (i.e. to the peak current) where the electron-laser interaction takes place. Since an increase of the beam current induces a bunch lengthening via potential well distortion, this electronic density cannot be assumed proportional to the whole beam current. A very satisfying numerical fit is obtained using a quadratic function, as expected regarding the analytical model: $I_{coh} = I_{und} N_e^2 f_n^2 J_n^2(n\Delta\alpha)$, confirming the coherence of the enhanced third harmonic.

4.3 Observation of coherent synchrotron radiation

While performing CHG experiments, bursts of TeraHertz radiation from CSR were observed at the BL6B beam line [53]. CSR occurs when the electron bunch is smaller than the radiated wavelength. This configuration can be achieved in two different modes: first, by creating micro structures in the longitudinal electronic density distribution using for instance a short laser pulse in the slicing mode, second, by reducing drastically the bunch length using low momentum compaction factor α_c. In turn, in this low α_c mode, two different regimes of THz radiation

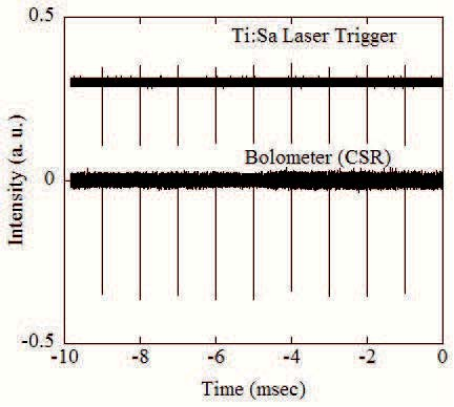

Fig. 10. THz pulses induced by the laser injection. The lower curve is the output signal of the TeraHertz detector, the Bolometer, and the upper curve the laser trigger signal. The THz radiation is collected at the output of the second bending magnet after the OK using a magic mirror [56] which focuses the source but also reduces the time delay due to the large acceptance: the summation of the optical path length and the electron orbital length is the same for each emitting position. THz detector is a liquid Helium cooled InSb Bolometer (QMC Instruments LTD, QFI/2(LF/MF) Special), sensitive from 0.2 to 3 mm with a few μs temporal resolution.

generation have been demonstrated [54]: the steady-state and the burst mode. Steady-state allows small intensity fluctuations and a peaked spectrum, the machine being operated in multibunch filling. In contrast, in the burst mode, partial filling allows higher peak current leading to more intense but fluctuating intensity, and broader spectrum. Two of those three modes have been successfully tested at UVSOR-II: without laser injection in burst mode [13], and using the femtosecond infrared laser in the slicing mode [50,55] (see Fig. 10). In the slicing mode, the microbunching induced by the laser occurs in the first part of the OK, and therefore uses the same set-up for laser transport as the CHG experiment. The THz radiation is collected at the output of the second bending magnet after the OK and sent to a THz detector.

It is possible at UVSOR-II to generate simultaneously UV and THz radiations both resulting from the electron-laser interaction in the optical klystron.

4.4 Pulse length and spectral width

In order to investigate the coherence of the enhanced radiation, the pulse lengths of the third harmonic and of the spontaneous emission have been measured with the double sweep streak camera (see Fig. 11). The width of the spontaneous emission is 91 ps-rms, whereas the width of the coherent emission is significantly shorter: 3 ps-rms, close to the typical streak camera resolution in this time scale mode of operation: 2 ps-rms. Deconvolution leads to a pulse length of 2.3 ps-rms for the third coherent harmonic, still limited by the resolution of the detector. This is an evidence of pulse length reduction in CHG, an evolution towards higher temporal coherence.

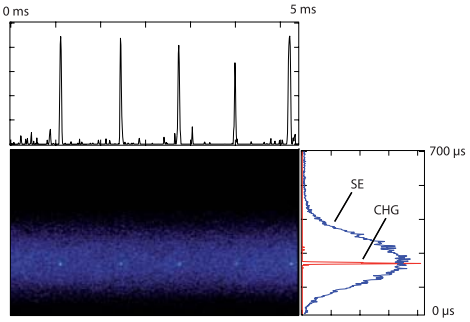

Fig. 11. Electron bunch emission vs. time, measured with the double sweep streak camera. The bright spots correspond to the emission of the laser heated electron bunch, and continuous background to unheated bunch emission, i.e. spontaneous emission. Pulse length is deduced from the vertical profiles. Full scales are 5 ms for the horizontal and 700 ps for the vertical axis.

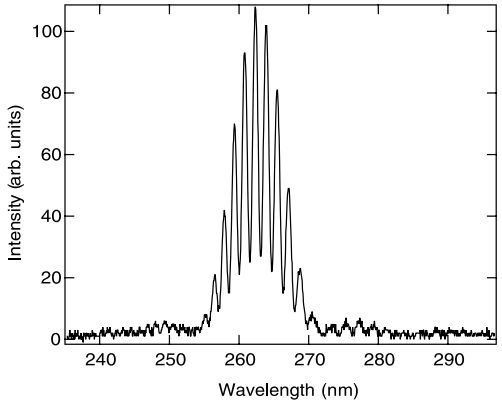

Fig. 12. Spectrum of the spontaneous emission around 266 nm, performed with the spectrometer (see Fig. 1). Undulator gap = 40.8 mm.

The spectral width of the spontaneous emission around 266 nm was first measured using a high resolution spectrometer (see Fig. 12). It is 9.4 nm (in agreement with the 9.8 nm theoretical value). The most intense fringe is at 262 nm with 0.92 nm-FWHM width. Because the spectrometer could not be triggered on the laser signal, a monochromator was used to measure spectra of the coherent third harmonic (see Fig. 13). Seeding with 0.5 W average power, and 185 fs pulse duration, the spectral width is less than 2 nm-FWHM, and than 2.2 nm seeding with 1 W and 560 fs.

Since the electrons radiating coherently are confined within the laser pulse length, the coherence length of the coherent third harmonic can be assumed equal to the laser pulse one. The bandwidth of the third harmonic corresponding to a Fourier-transformed 185 fs rectangular pulse is 1.14 nm-FWHM.

Coherent emission resulting from the interference of a train of microbunches, the spectral width can also be approximated using the one dimension grating model [35] $\delta\lambda_c = \lambda_L^2/(2n^2\sqrt{\pi}\sigma_{Laser})$, where σ_{Laser} is the length of the train, i.e. the laser pulse length, and n the harmonic

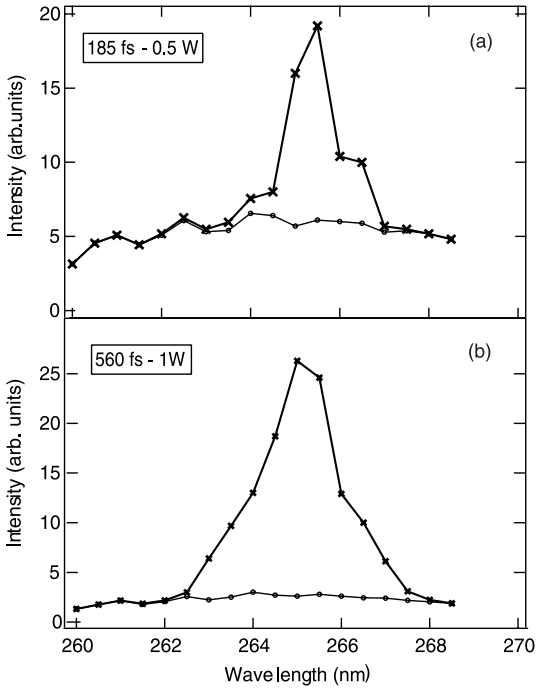

Fig. 13. Intensity of the bunch emission around 266 nm vs. wavelength. Electron bunch emission (×) with laser heating, (•) without laser heating. (a) $P_{Laser} = 0.5$ W, pulse duration = 180 fs, (b) $P_{Laser} = 1$ W, pulse duration = 560 fs. The radiation is collected at the output of the OK, and sent through a monochromator (Shimazu, SPG-120) with a resolution of 2.5 nm (measured using a Hg lamp at 254 nm) followed by the photomultiplier. Undulator gap = 40.8 mm; $I = 0.8$ mA.

number. This expression leads to 0.36 nm width using a 185 fs-fwhm pulse duration.

The simulated spectral width depends on the seeding laser pulse duration, and average power. Seeding with 0.5 W average power and 1200 fs, the third harmonic bandwidth is 0.22 nm-FWHM. Using shorter seeding laser pulse duration, 200 fs, at the same average power, increases the bandwidth up to 1.46 nm-FWHM.

Both analytical expressions and simulation predict a bandwidth below 1.5 nm. Such narrowing of the third harmonic spectrum could not be measured because of the lack of appropriate detection. Nevertheless, a clear reduction (from 10 to 2 nm) of the spectral bandwidth induced by the laser seeding has been observed.

Coherent Harmonic Generation lead to both spectral and temporal narrowing of the radiation on the third harmonic of the fundamental. With a 0.92 nm-FWHM spectral width (considering one fringe of the spontaneous emission spectrum) and 188 ps-FWHM bunch length, the spontaneous emission is 1.6×10^3 times above the Fourier limit. With a 2.5 nm-FWHM spectral width and a 5.4 ps-FWHM pulse length, the coherent third harmonic is at least ten times closer to the Fourier limit than spontaneous emission. More accurate measurements (autocorrelation for pulse duration, higher resolution monochromator for spectral width) may help in getting closer to actual values, and therefore to theoretical expectations.

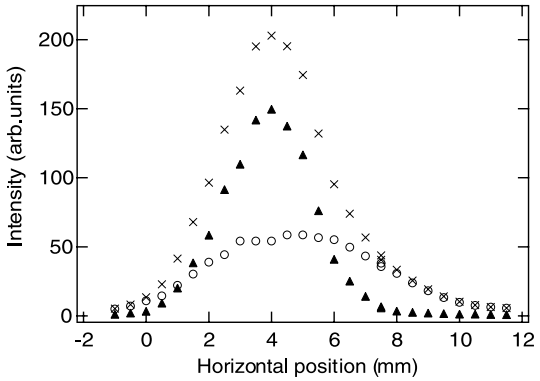

Fig. 14. Horizontal profile of the radiation at the output of the optical klystron: 21 cm after the vacuum chamber. (○) unheated bunch emission, (×) heated bunch emission, (▲) difference between heated and unheated bunch signals. The measurement was performed using a slit of 0.9 mm width and 31 mm height, mounted on a micrometric translation stage. $I = 2.7$–2.3 mA, $P_{Laser} = 1.77$ W, $\Delta T_{Laser} = 0.6$ ps.

In terms of brightness, an enhancement by factor 4000 from spontaneous emission to CHG is obtained: an optimised CHG experiment can result in an attractive light source for storage ring users.

4.5 Horizontal dimension

The horizontal profile of the third harmonic is given in Figure 14. The laser injection reduces the width of the profiles from 2.7 down to 1.6 mm. The laser beam does not fully overlap the electron beam in the transverse plane: due to the strong vertical focusing of the optics in the OK, laser beam is smaller in the horizontal dimension. This narrowing of the coherent third harmonic width is a consequence of the limited interaction distance in the horizontal dimension (compared to the spontaneous emission). Spatial coherence measurement of the radiation is foreseen, since the third coherent harmonic should also benefit from the spatial coherence of the seed laser.

5 Influence of the laser parameters on CHG

To further characterize the harmonic generation using an external seed, the influence of several laser parameters has been studied.

5.1 Resonant wavelength

The resonant wavelength λ_R of the OK is set by the gap in the undulators. The coherent third harmonic can be detected for varying gaps from 40.1 mm aperture up to 41.7 mm, with a maximum at 40.7 mm as illustrated in Figure 15. Since the enhancement of the coherent harmonics requires that the resonant wavelength matches the modulation wavelength, i.e. the seed laser wavelength,

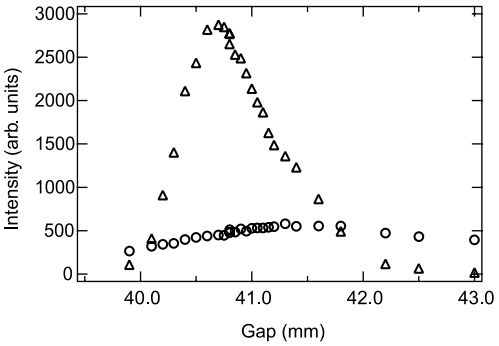

Fig. 15. PM signal vs. gap. (△) CHG, (○) SR. P_{Laser} = 1.12 W, Φ_{Laser} = 11.5 mm, ΔT_{Laser} = 1.12 ps. Normalization at I_{Beam} = 2.35 mA.

Table 5. Resonance wavelength of spontaneous emission measured for various undulator gap values using the spectra of spontaneous emission at the output of the OK. The undulator parameter K is being calculated using $K = \sqrt{4\gamma^2(\lambda_R/\lambda_0) - 2}$.

Gap (mm)	λ_R (nm)	K (λ_R)
39.8	806	6.19
40.0	798	6.16
40.8	773	6.06
41.2	755	5.98
41.4	752	5.97

large detuning of the gap destroys the microbunching and therefore the coherent emission.

According to resonant wavelength measurements corresponding to various gaps around 40.7 mm (see Tab. 5), the resonant wavelength optimizing the coherent emission is λ_R = 773 nm, 30 nm less than the expected value, i.e. the laser wavelength. Such phenomenon has been previously described and explained [60] considering a Gaussian mode for the optical waves, instead of the usually assumed plane-wave.

Indeed, using the cylindrical coordinates r and z, the electromagnetic wave in fundamental Gaussian mode is given by:

$$E(r,z) = \frac{E_0}{w(z)} \exp\left(i(kz - \eta(z)) - \left(\frac{r}{w_0 w}\right)^2 - i\frac{k}{2R(z)}\right), \tag{13}$$

where $w^2(z) = 1 + (z/Z_0)^2$, $R(z) = z + Z_0^2/z$, $\eta(z) = \tan^{-1}(z/Z_0)$, $Z_0 = \pi w_0^2/\lambda_L$ is the Rayleigh length, w_0 the beam waist, $k = 2\pi/\lambda$ the carrier wave number, and E_0 the electric field amplitude. The expression of the energy exchange E_{ex} along the undulator is given by the following equation:

$$E_{ex} = \int \frac{e\boldsymbol{\beta}}{\beta_z} \cdot \boldsymbol{E} dz = \int dz \frac{\cos\left(\frac{2\pi\Delta\lambda}{\lambda\lambda_0} z - \frac{1}{\tan(z/Z_0)} + \Phi\right)}{\sqrt{1 + (z/Z_0)^2}}, \tag{14}$$

$\boldsymbol{\beta}$ being the electrons velocity. At resonance, this term is either maximum or minimum. In the case of a plane wave ($w(z) = 1$ and $\eta(z) = 0$), the optimum is obtained for the well known resonant wavelength: $\lambda_R = (\lambda_0/2\gamma^2)(1+K^2/2)$. Assuming a Gaussian mode, the optimum is reached for a different wavelength $\lambda_R + \Delta\lambda$, which analytical expression is not straightforward. Since modulation is assumed to occur in the first part of the optical klystron, the integration is performed along the modulator. Using the parameters given in Table 2, a Rayleigh length Z_0 = 0.24 m and focusing 0.2 m inside the modulator, maximum energy exchange E_{ex} is obtained for λ_R = 768 nm, in good agreement with the experimental value.

Seeding with an external laser focused in the modulator, leads to a new definition of the resonant wavelength, taking into account the Gaussian mode of the seeded electromagnetic field. Nevertheless, the output radiation is still centered on the third harmonic of the laser, at 266 nm (see Fig. 13).

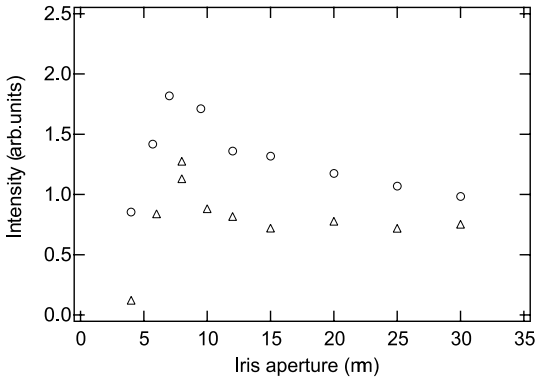

Fig. 16. PM signal vs. iris aperture. (△) P_{Laser} = 1.6 W, (○) P_{Laser} = 0.8 W, ΔT_{Laser} = 812 ps.

5.2 CHG intensity output

The coherent harmonic intensity revealed to be strongly dependent on several seed laser parameters such as iris aperture, pulse duration and input power, as expected regarding both numerical and analytical models.

5.2.1 Laser diameter influence

Varying the iris aperture from 30 mm up to 4 mm, we observed a strong increase of the third coherent harmonic signal followed by a decrease for too small aperture size (see Fig. 16). With both laser power used, the optimal aperture size was 7 mm.

Calculation of the coherent intensity with the analytical model as a function of the waist (required in the peak power evaluation) also revealed an optimum around 200 μm, corresponding to the measured waist without iris.

Closing a diaphragm placed before the focusing lens means both decreasing the laser energy and increasing the focal spot size, therefore quickly decreasing the focal intensity. The enhancement of the harmonic signal by a factor 2 from total initial injection, is the consequence of a balance between several laser parameters: injected average power,

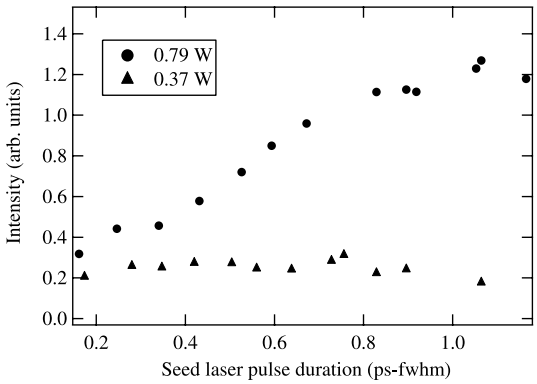

Fig. 17. Coherent emission vs. pulse duration. (•) P_{Laser} = 0.79 W, (▲) $P_{Laser} = 0.37$ W, $\Phi_{Laser} = 8$ mm.

and so peak power, transverse dimensions, focusing and intensity inside the modulator.

5.2.2 Laser pulse duration influence

The laser pulse duration can be tuned from nominal value (130 fs) up to 1.2 ps by changing the chirp of the pulse with a set of gratings. With 0.79 W average power, the longer the laser pulse, the more intense the coherent third harmonic, whereas the spontaneous emission remains at constant intensity (see Fig. 17). At lower power (0.37 W) the third harmonic signal remains flat.

Such tendency is reproducible using the analytical model. However, the coherent emission calculated is found extremely sensitive to those parameters. The analytical model helped understanding the basic steps of harmonic generation, the bunch lengthening, as well as the quadratic dependency on the peak current. Still, because the laser intensity longitudinal profile is not considered, the strength of the photon-electron interaction is overestimated, and disables smoothing of this interaction on the edges of the laser distribution, resulting in an unrealistic sensitivity to the laser parameters. In addition, since those laser parameters are arguments of a Bessel function, this sensitivity often leads to fast annihilation of the coherent intensity. The simulation tool PERSEO, which models the laser and electron bunch longitudinal distributions, is found in better agreement with the experimental results (see Fig. 18). At "high" power (above 0.7 W) the simulated third harmonic intensity increases with the seeding laser pulse duration. At 0.5 W, as in the experiment, it is nearly flat versus pulse duration (slow increase followed by decrease) and even slowly decreases with pulse duration at 0.2 W.

In addition, simulations revealed that coherent emission is located along the laser-electron beam interaction region where the bunching coefficient approximately equals 0.2 on the fundamental. Over 0.3, and below 0.1, the harmonic signal remains low. At a given average power, an increase of the pulse duration involves more electrons in the interaction, and leads to more coherent harmonic generation, until the local electric field becomes too low to bunch at higher value than 0.1.

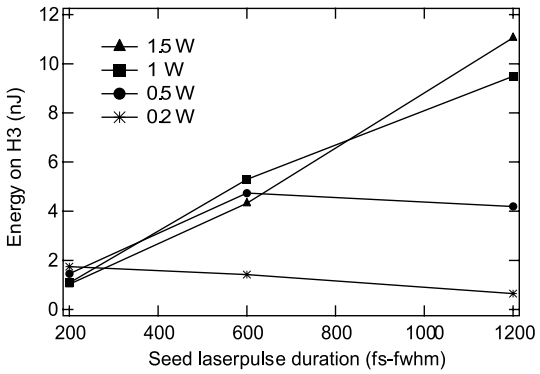

Fig. 18. Coherent emission vs. laser pulse duration. Simulation with PERSEO. (▲) $P_{Laser} = 1.5$ W, (■) $P_{Laser} = 1$ W, (•) $P_{Laser} = 0.5$ W, (∗) $P_{Laser} = 0.2$ W. Parameters: $\sigma_\gamma = 4.2 \times 10^{-4}$, and parameters of Tables 1–3. The matching with the experimental results has been obtained using a slice normalized emittance of $\epsilon_n = 1$ mm mrad, corresponding to a beam surface in the transverse plane of 4.8×10^{-8} m^2, half of the assumed surface on UVSOR-II storage ring. The mismatch in the beams dimensions prevents the edges of the electronic distribution in the transverse plane to be microbunched, and therefore to perform coherent emission. This mismatch is taken into account in PERSEO reducing the transverse sizes of the electron beam for a given peak current.

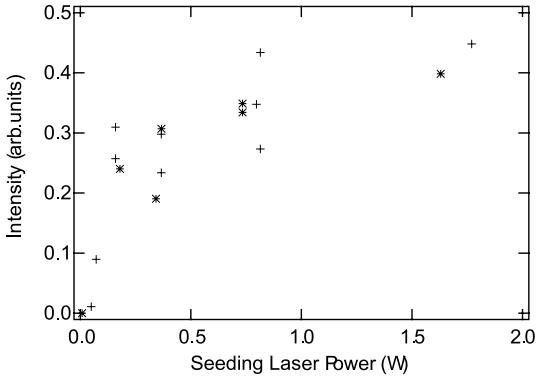

Fig. 19. Coherent emission versus seeding laser average power. Variation of the laser average power is obtained using a set of neutral densities. $\Phi_{Laser} = 8$ mm, (+) $\Delta T_{Laser} = 160$ fs, (∗) $\Delta T_{Laser} = 157$ fs.

5.2.3 Laser energy influence

The third harmonic intensity was finally studied as a function of the seed laser average power (see Fig. 19). According to the experiment, the higher the seeding power, the more intense the coherent harmonic. Using a stronger electric field enables more efficient bunching in the modulator, leading to higher coherent intensity in the radiator.

The simulated coherent harmonic using similar pulse duration decreases with the input power. Increase is obtained with longer pulse durations (see Fig. 20). Indeed, at 1200 ps, simulated tendency is similar to the experimental one. This simulation/experiment difference may

Highlight Paper

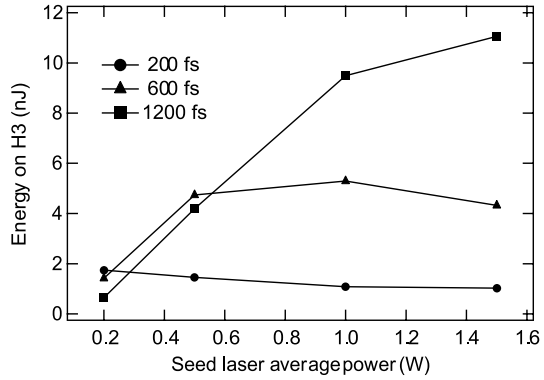

Fig. 20. Coherent emission versus seeding laser average power. Simulation with PERSEO. (■) $\Delta T_{laser} = 1200$ fs, (▲) $\Delta T_{laser} = 600$ fs, (•) $\Delta T_{laser} = 200$ fs. $\sigma_{gamma} = 4.2 \times 10^{-4}$, $\epsilon_n = 1$ mm mrad. The other parameters are the experimental parameters presented in Tables 1–3.

be explained by the lack of experimental precise transverse overlap measurements.

Comparison between experimental results and simulations under several parameters allowed further understanding of the process. Similar investigations should be performed regarding the whole coherence dependency (spectrum and pulse length) of the third harmonic versus seed laser parameters.

6 Conclusion

In summary, coherent harmonic generation has been performed on UVSOR-II storage ring, seeding a femtosecond infra-red laser. Spectral and temporal narrowing of the third harmonic of the undulator has been observed, as well as an intensity enhancement with respect to the spontaneous emission. We also reported simultaneous generation of TeraHertz radiation, using CSR effect, and UV radiation, using CHG, on UVSOR-II facility: an unusual set-up of great interest for many users experiments.

Among the foreseen CHG experiments at UVSOR-II, is observation of the fifth harmonic using an under vacuum monochromator. Further investigations will also aim at characterizing experimentally more accurately the dynamics (refreshment) of the electron bunch within two laser shots and at performing detailed simulations on the relaxation of the heated electrons both for CHG and slicing. Additional experiments are planned for refining the coherence properties with a gating of the harmonic pulse for spectra and pulse duration measurements. In addition, since the UVSOR-II FEL oscillator [61] can deliver significant power from 215 up to 800 nm, internal seeding configuration could be tested and performances compared to external seeding. Finally, odd harmonic generation [62] is foreseen. Reducing the electron beam energy down to 515 MeV, the modulator and radiator can be tuned at the fundamental wavelength of infra-red laser in the helical mode. In this configuration, the radiator can enhance odd harmonics of the fundamental so that observation of the second and fourth harmonics (400 and 200 nm) is expected.

We are thankful to J. Yamazaki for the set-up of the experiment, to S. Kimura for the use of the infra red line, to C. Bruni and B. Carré for their helpful advises. A part of this work was supported by Grant-in-Aid for Scientific Research of JSPS and by International Collaboration Program of IMS.

References

1. S. Takemoto, J. Yang, T. Kondoh, Y. Yoshida, EPAC'06 Conference, 2511 (2006)
2. G.L. Carr, M.C. Martin, W.R. McKinney, K. Jordan, G.R. Neil, G.P. Williams, Nature **420**, 153 (2002)
3. P. Sprangle et al., J. Appl. Phys. **72**, 5032 (1992)
4. R.W. Schoelein, W.P. Leemans, A.H. Chin, P. Volfbeyn, T.E. Glover, P. Balling, M. Zolotorev, K.J. Kim, S. Chattopadhyay, C.V. Shank, Science **287**, 2237 (2000)
5. H. Ohkuma, M. Shoji, S. Suzuki, K. Tamura, T. Yorita, K. Nakayama, S. Okajima, Y. Arimoto, K. Kawase, M. Fujiwara, EPAC'06 Conference, 961 (2006)
6. `www.esrf.eu/UsersAndScience/Experiments/CRG/BM07`
7. A.A. Zholents, M.S. Zolotorev, Phys. Rev. Lett. **76**, 912 (1996)
8. R.W. Schoenlein, S. Chattopdhyay, H.H.W. Chong, T.E. Glover, P.A. Heimann, C.V. Shank, A.A. Zholents, M.S. Zolotorev, Science **287**, 2237 (2000)
9. J.B. Murphy, S. Krinsky, Nucl. Instrum. Meth. Phys. Res. A **346**, 571 (1994)
10. F. Wang et al., Phys. Rev. Lett. **96**, 064801 (2006)
11. K. Holldack, S. Khan, R. Mitzner, T. Quast, Phys. Rev. Lett. **96**, 054801 (2006)
12. W.C. Barry et al., EPAC'02 Conference, 656 (2002)
13. A. Mochihashi, M. Hosaka, M. Katoh, M. Shimada, S. Kimura, Y. Takashima, T. Takahashi, EPAC'06 Conference, 3382 (2006)
14. D.A.G. Deacon, L.R. Elias, J.M.J. Madey, G.J. Ramian, H.A. Schwettman, T.I. Smith, Phys. Rev. Lett. **38**, 892 (1977)
15. L.R. Elias, IEEE J. Quant. Electron **QE23** (1987)
16. B. Faatz, FEL'06 Conference, 23 (2006)
17. L.R. Elias, W.M. Fairbank, J.M.J. Madey, H.A. Schwettman, T.I. Smith, Phys. Rev. Lett. **36**, 717 (1976)
18. B. Bonifacio, N. Narducci, C. Pellegrini, Opt. Commun. **50**, 373 (1984)
19. P.L. Csonka, Part Acc. **8**, 225 (1978); N.A. Vinokurov, A.N. Skrinsky, Preprint 77-88, Nuclear Physics Institute of Novossibirsk (1978)
20. R.R. Freeman, B.M. Kincaid, AIP Conference Proceedings **119**, 277 (1984)
21. R. Coïsson, F. De Martini, Phys. of Quant. Electron. **9**, 939 (Addison-Wesley, 1982)
22. C.A. Brau, *Free Electron Lasers* (Academic Press, New York, 1990); W.B. Colson, A.M. Sessler, Ann. Rev. Nuc. Part. Sci. **35**, 25 (1985); H.P. Freund, R.K. Parker, *Free Electron Lasers in Encyclopedia of Physical Science and Technology 1991 Yearbook* (Academic Press, New York, 1991)

23. G. Lambert, B. Carré, M.E. Couprie, D. Garzella, A. Doria, L. Giannessi, T. Hara, H. Kitamura, T. Shintake, FEL'04 Conference, 363 (2004)
24. L.H. Yu et al., Phys. Rev. A **44**, 5178 (1991)
25. R. Prazeres, J.M. Ortega, C. Bazin, M. Bergher, M. Billardon, M.E. Couprie, M. Velgue, Y. Petroff, Nucl. Inst. Meth. A **272**, 68 (1988)
26. N.A. Vinokurov, A.N. Skrinsky, Preprint 77-59, Nuclear Physics Institute of Novossibirsk (1977)
27. R. Prazeres, P. Guyot-Sionnest, J.M. Ortega, D. Jaroszynski, M. Billardon, M.E. Couprie, M. Velghe, Y. Petroff, Nucl. Inst. Meth. A **304**, 72 (1991)
28. L.H. Yu, A. Doyuran, L. DiMauro, W.S. Graves, E.D. Johnson, R. Heese, S. Krinsky, H. Loos, J.B. Murphy, G. Rakowsky, J. Rose, T. Shaftan, B. Sheehy, J. Skaritka, X.J. Wang, Z. Wu, Nucl. Inst. Meth. A **528**, 436 (2004)
29. L. Wen, R.R. Lucchese, A. Doyuran, W. Zilu, H. Loos, G.E. Hall, A.G. Suits, Phys. Rev. Lett. **92**, 083002 (2004)
30. V. Litvinenko, Nucl. Inst. Meth. A **507**, 265 (2003)
31. G. De Ninno, M.B. Danailov, B. Diviacco, M. Ferianis, M. Trovo, FEL'04 Conference, 237 (2004)
32. F. Curbis, G. De Ninno, FEL'05 Conference, 459 (2005)
33. M. Katoh, M. Hosaka, A. Mochihashi, J. Yamazaki, K. Hayashi, Y. Hori, T. Honda, K. Haga, Y. Takashima, T. Koseki, S. Koda, H. Kitamura, T. Hara, T. Tanaka, AIP'04 **708**, 49 (2004)
34. P. Elleaume, J. Phys. (Paris) **44(C1)**, 353 (1983)
35. R. Prazeres, Ph.D. thesis, University of Paris XI, Orsay, 1988, Chap. 2-3, pp. 27–71
36. W. Colson, *Laser Handbook: Free Electron Lasers* (North Holland Publisher, Amsterdam, 1990), Vol. 6, Chap. 5
37. W. Colson, P. Elleaume, Appl. Phys. B **29**, 101 (1982)
38. D. Nutarelli, Ph.D. thesis (University of Paris XI, Orsay, 2000), Chap. 1, pp. 46–50
39. J.M.J. Madey, J. Appl. Phys. **42**, 1906 (1971)
40. M. Pessot, P. Maine, G. Mouroux, Opt. Commun. **62**, 419 (1987); P. Maine, B. Strickland, P. Bado, M. Pessot, G. Mouroux, IEEE J. QE **24**, 398 (1988)
41. G. De Ninno, M.E. Couprie, D. Nutarelli, D. Garzella, E. Renault, M. Billardon, Phys. Rev. E **64**, 026502 (2001)
42. See `www.perseo.enea.it`
43. W.B. Colson, G. Dattoli, F. Ciocci, Phys. Rev. A **31**, 828 (1985)
44. M. Hosaka, M. Katoh, A. Mochihashi, J. Yamasaki, K. Hayashi, Y. Takashima, Nucl. Inst. Meth. A **528**, 291 (2004)
45. G. Dattoli, L. Mezi, M. Migliorati, A. Renieri, M.E. Couprie, D. Garzella, D. Nutarelli, C. Thomas, G. DeNinno, R. Walker, Nucl. Inst. Meth. A **471**, 403 (2001)
46. A. Lin, H. Hama, S. Takano, G. Isoyama, Jpn J. Appl. Phys. **31**, 921 (1992)
47. H. Hama, Nucl. Instr. Meth. A **375**, 57 (1996)
48. H. Hama, K. Kimura, M. Hosaka, J. Yamazaki, T. Kinishita, Nucl. Instr. Meth. A **393**, 23 (1997)
49. H.P. Freund, P.G. ÕShea, S.G. Biedron, Phys. Rev. Lett. **94**, 074802 (2005)
50. M. Katoh, M. Hosaka, S. Kimura, A. Mochihashi, M. Shimada, T. Takahashi, Y. Takashima, T. Hara, EPAC'06 Conference, 3377 (2006)
    M. Katoh, M. Hosaka, A. Mochihashi, S. Kimura, Y. Takashima, T. Takahashi, to be published in the Proceedings of SRI 2006, Abstract No. 11030015
51. M. Sands, The physics of Electron Storage Rings. An introduction (1971)
52. T. Tanaka, H. Kitamura, SPring-8/RIKEN, `http://radiant.harima.riken.go.jp/spectra/getstart.html`
53. S. Kimura, E. Nakamura, T. Nishi, Y. Sakurai, K. Hayashi, J. Yamazaki, M. Katoh, Infrared Physics and Technology **49**, 147 (2006)
54. M. Abo-Bakr, J. Feikes, K. Holldack, G. Wüstefeld, Phys. Rev. Lett. **88**, 254801 (2002)
55. M. Hosaka et al., Jpn J. Appl. Phys. (submitted)
56. R. Lopez-Delgado, H. Szwarc, Opt. Commun. **19**, 286 (1976)
57. K. Holldack, T. Kachel, S. Khan, R. Mitzner, T. Quast, Phys. Rev. Special Topics A and B **8**, 040704 (2005)
58. R.W. Schoenlein, S. Chattopadhyay, H.H.W. Chong, T.E. Glover, P.A. Heimann, C.V. Shank, A.A. Zholents, M.S. Zolotorev, Science **287** (2000)
59. A. Amir, Y. Greenzweig, Phys. Rev. A **34**, 4809 (1986)
60. W.B. Colson, P. Elleaume, Appl. Phys. B **29**, 101 (1982)
61. M. Katoh, M. Hosaka, A. Mochihashi, M. Shimada, T. Hara, J. Yamazaki, K. Hayashi, EPAC'06 Conference, 3374 (2006)
62. H.P. Freund, Private Communication, August 2006